Fast Computation of Layered Medium Green's Functions of Multilayers and Lossy Media Using Fast All-Modes Method and Numerical Modified Steepest Descent Path Method

Boping Wu, *Student Member, IEEE*, and Leung Tsang, *Fellow, IEEE*

***Abstract*—A fast and accurate approach, based on the fast all-modes method (FAM) and the numerical modified steepest descent path method (NMSP), was previously used to calculate the spatial Green's function for a single-layer lossless dielectric medium over a perfect electric conductor. This paper successfully extends that approach to two new cases. The first is the multilayer case where the medium has an arbitrary number of layers. The second is lossy media over an imperfect conductor. The FAM locates all modes accurately on the complex plane. The modes include surface wave modes, leaky wave modes, and improper modes. For a typical six-layer case over a ground plane, the FAM requires only 2.265 s of pre-processing that includes computing 200 mode locations by using a P4 3.2-GHz PC with MATLAB. The NMSP is then used to evaluate the steepest descent path integral. Accuracy within 0.2% is achieved in comparison with the benchmark calculations. Within this context of accuracy, the total CPU per distance point is less than 7.6 ms for distances larger than 0.02 free-space wavelength and is less than 2.7 ms for distances larger than two free-space wavelengths. This method is shown to be fast and accurate, even for large-distance interactions in the multilayer and lossy media.**

***Index Terms*—Fast all-modes method (FAM), Green's functions, layered media, numerical modified steepest descent path method (NMSP).**

I. Introduction

THE evaluation of the spatial Green's functions of a multilayered media is an indispensable step when implementing the method of moments (MoM) for various applications such as microstrip interconnects and antennas [2], [3], geophysical prospecting, remote sensing, etc. It is well known that the conventional Sommerfeld integration path (SIP) representation of a layered medium Green's function is poorly convergent due to the highly oscillatory behavior of the integrands along the SIP. Methods have been developed to efficiently compute the Sommerfeld integrals. For example, the rational function fitting method [4], [5], [22] uses the spectral-domain representations to obtain closed-form expressions of the spatial-domain Green's functions. In [5], the algebraic decay of the integrand is accounted for by rational-fitting approximations. On the other hand, several improvements have been made on the discrete complex image method [6]–[9], which approximates the spectral-domain Green's functions by a sum of exponentials. The paths of integration in the discrete complex image method are only a small deformation from the SIP. Such that the asymptotic decay of the integrand is still algebraic. In certain circumstances, it may require large CPU time to calculate the summations or images for error correction even with the extraction of the singularity poles.

In our recent research, we used the numerical modified steepest descent path method (NMSP) combined with the fast all-modes method (FAM) to solve the spatial Green's functions for a single-layer lossless medium over a perfect electric conductor (PEC) [1], [10], [11].

In this paper, we extend the FAM/NMSP method to compute the layered medium Green's functions of multilayers. We also extend the FAM/NMSP method to the lossy case. The FAM/NMSP method works for all distance ranges. The NMSP can integrate along the steepest descent path (SDP) using minimal CPU time by sampling only a few integration points after the extraction of the nearby singularity poles. This is because of the following.

- The SDP eliminates the fast oscillation of the space-dependent part inside the integrand.
- The asymptotic decay of the integrand on the SDP is exponential rather than algebraic even when both source and field points are on the same interface.
- The space-independent part of the integrand on the SDP is smoothened by extracting all the nearby poles.

In the past, some numerical methods for locating the zeros of an analytic function have been proposed [12]–[16], [21]. However, the method in [16] converges poorly and requires large CPU for locating merely ten poles. The method may even miss important poles. On the other hand, the FAM utilizes the special property of layered medium Green's function that there are no branch points for the complex wavenumbers k_{iz}'s of the intermediate layers, and is able to find every root accurately on the entire complex plane. For single-layer media [1], it was shown that the FAM can locate hundreds of modes within seconds.

For the multilayered problem, the expression of the reflection coefficient is not as straightforward as that of the single-layer case. In Section II-A, we demonstrate that, in spite of the complicated reflection coefficients of the multilayer case, all mode

Manuscript received November 2, 2007; revised February 1, 2008.

The authors are with the Department of Electrical Engineering, University of Washington, Seattle, WA 98195 USA (e-mail: bennywu@u.washington.edu; tsang@ee.washington.edu).

Color versions of one or more of the figures in this paper are available online at http://ieeexplore.ieee.org.

Digital Object Identifier 10.1109/TMTT.2008.923901

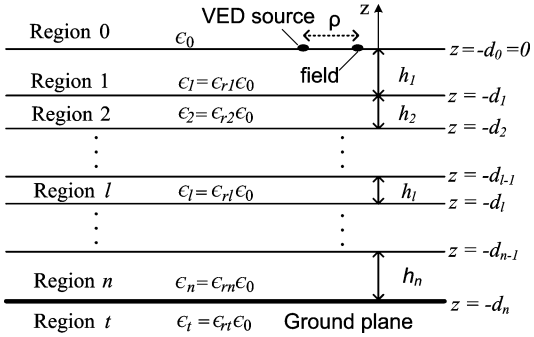

Fig. 1. VED source above a lossy dielectric substrate of multilayers over the GND.

locations can still be found accurately within seconds by using the determinant format for the Taylor-series expansions. A general systematic algorithm is also provided for layered medium with an arbitrary number of layers above an imperfect ground plane (GND).

In Section II-B, the NMSP is implemented to perform the integration efficiently since the integral along the SDP is smoothened by subtracting all the poles close to the saddle point. The pole proximities are accounted for by using incomplete error functions [17]. The Green's functions are finally evaluated by summing the contribution of the SDP together with the residues of both surface wave modes and leaky wave modes.

In Section III, we illustrate the numerical results of the FAM/NMSP method for three typical dielectric substrates, including two difficult situations. The first situation is the surface field when both source and field points are on the surface, so that the integrand is least convergent. The second situation is the lossy case, in which the surface wave modes no longer dominate in the far–field region. Accuracy within 0.2% is achieved in comparison with the benchmark calculations of our previous half-space extraction method [18]. Such accuracy is necessary for impedance matrix elements calculation of the MoM in most layered media applications. The required CPU of computing the layered medium Green's function is dependent on the required accuracy. We tabulate the CPU within the context of the above accuracy. The FAM/NMSP method is shown to be fast and accurate. We have not compared the CPU with other methods, as there is no general agreement on how to make fair comparisons. We also tabulate the number of surface wave modes, leaky wave modes, the number of poles for extraction, and the number of points for trapezoidal integration as a function of distance.

II. Spatial Green's Function of Vertical Electric Dipoles (VEDs)

Consider a VED placed at the origin above a multilayered media consisting of N dielectric substrate layers and a GND at the bottom, as shown in Fig. 1. A component of the dyadic Green's function of layered media is the vertical component of the electric field E_{0z}. The electric field E_{0z} on the surface of the top interface ($z = -d_0 = 0$) is

$$E_{0z}(\rho) = -\frac{Il}{8\pi\omega\varepsilon_0}\int_{-\infty}^{\infty} dk_\rho (1+R^{\mathrm{TM}})\frac{k_\rho^3}{k_{0z}}H_0^{(2)}(k_\rho\rho) \quad (1)$$

where $k_0 = 2\pi/\lambda_0$, $k_{0z} = \sqrt{k_0^2 - k_\rho^2}$, λ_0 is the wavelength in region 0, ρ is the source-to-field distance on the horizontal plane, and R^{TM} is the TM reflection coefficient for the multilayered media. The convergence of the Sommerfeld integral in (1) was discussed in [1]. Once the surface field is solved for both the source point and the field point on the surface, problems for other locations of sources and receivers are much easier to handle because the SDP is shifted.

A. Fast All-Modes Determination in the Complex Plane

The FAM was previously used for the single-layer case [1], [11]. This was based on the simple mode equation for the single-layer case. In this paper, we formulate the mode equation in the determinant format, also called Cramer's rule. This reformulation subsequently allows the method to be extended to the medium with an arbitrary number of layers. We will firstly present two complementary methods for locating all the modes for a two-layer lossless dielectric substrate above a PEC. We will then describe the approach for solving the lossy dielectric substrate above an imperfect conductor. Finally, we will discuss the method for solving the medium with an arbitrary number of layers above an imperfect conductor.

The electric field and magnetic field on the tangential direction are presented for each region as follows. Note that we use sine and cosine functions instead of the exponential functions to present the electric and magnetic field in each intermediate region.

Region 0:

$$E_{0\rho}(\rho) = \frac{jIl}{8\pi\omega\varepsilon_0}\int_{-\infty}^{\infty} dk_\rho[\exp(jk_{0z}z) - R^{\mathrm{TM}}\exp(-jk_{0z}z)] \cdot k_\rho^2 H_1^{(2)}(k_\rho\rho) \quad (2)$$

$$H_{0\phi}(\rho) = -\frac{jIl}{8\pi}\int_{-\infty}^{\infty} dk_\rho[\exp(jk_{0z}z) + R^{\mathrm{TM}}\exp(-jk_{0z}z)] \cdot \frac{k_\rho^2}{k_{0z}}H_1^{(2)}(k_\rho\rho). \quad (3)$$

Region 1:

$$E_{1\rho}(\rho) = \frac{jIl}{8\pi\omega\varepsilon_1}\int_{-\infty}^{\infty} dk_\rho\{Aj\sin[k_{1z}(z+d_1)) + B\cos[k_{1z}(z+d_1)]\} \cdot \frac{k_{1z}k_\rho^2}{k_{0z}}H_1^{(2)}(k_\rho\rho) \quad (4)$$

$$H_{1\phi}(\rho) = -\frac{jIl}{8\pi}\int_{-\infty}^{\infty} dk_\rho\{A\cos[k_{1z}(z+d_1)] + Bj\sin[k_{1z}(z+d_1)]\} \cdot \frac{k_\rho^2}{k_{0z}}H_1^{(2)}(k_\rho\rho). \quad (5)$$

Region 2:

$$E_{2\rho}(\rho)=\frac{jIl}{8\pi\omega\varepsilon_2}\int_{-\infty}^{\infty}dk_\rho C j\sin[k_{2z}(z+d_2)]\frac{k_{2z}k_\rho^2}{k_{0z}}H_1^{(2)}(k_\rho\rho) \tag{6}$$

$$H_{2\phi}(\rho)=-\frac{jIl}{8\pi}\int_{-\infty}^{\infty}dk_\rho C\cos[k_{2z}(z+d_2)]\frac{k_\rho^2}{k_{0z}}H_1^{(2)}(k_\rho\rho). \tag{7}$$

In *Region 2*, the unknowns are reduced to only one because the tangential electric field component $E_{2\rho}$ is zero on the interface ($z=-d_2$) with a PEC. The use of sine and cosines highlights the fact that the integrand of the E-field is an even function of k_{iz} of every intermediate layer i. There are only branch cuts of the two outermost layers and none for the intermediate layers. Due to the even function property, we use Taylor-series expansion to transfer the sine and cosine functions into a polynomial equation of k_{0z} without any square root and find the exact roots of the polynomial mode equation. Also note that in the intermediate layer of layer 1, we use $z+d_1$ in the argument of sine and cosine instead of z because this simplifies the expression and also increases the accuracy of the Taylor-series calculation.

Matching the boundary conditions (continuous tangential E and tangential H) at the interface $-d_0$ and $-d_1$, we obtain the following four equations with four unknowns R^{TM}, A, B, and C:

$$\begin{cases} R^{\mathrm{TM}}-\cos(k_{1z}d_1)A-j\sin(k_{1z}d_1)B=-1 & (8)\\ \dfrac{k_{0z}}{\varepsilon_0}R^{\mathrm{TM}}+\dfrac{k_{1z}}{\varepsilon_1}j\sin(k_{1z}d_1)A & \\ \quad+\dfrac{k_{1z}}{\varepsilon_1}\cos(k_{1z}d_1)B=\dfrac{k_{0z}}{\varepsilon_0} & (9)\\ A-\cos[k_{2z}(d_2-d_1)]C=0 & (10)\\ \dfrac{k_{1z}}{\varepsilon_1}B-\dfrac{k_{2z}}{\varepsilon_2}j\sin[k_{2z}(d_2-d_1)]C=0 & (11)\end{cases}$$

where $k_{1z}=\sqrt{k_1^2-k_\rho^2}$ and $k_{2z}=\sqrt{k_2^2-k_\rho^2}$. We get the expression of the reflection coefficients R^{TM} in the determinant format

$$R^{\mathrm{TM}}=\frac{\det(N_m)}{\det(D_n)}=\frac{\det\begin{bmatrix}-1 & -\cos(b) & -j\sin(b) & 0\\ a & \dfrac{jb\sin(b)}{\varepsilon_{r1}} & \dfrac{b\cos(b)}{\varepsilon_{r1}} & 0\\ 0 & 1 & 0 & -\cos(d)\\ 0 & 0 & \dfrac{bh_2}{h_1\varepsilon_{r1}} & \dfrac{-jd\sin(d)}{\varepsilon_{r2}}\end{bmatrix}}{\det\begin{bmatrix}1 & -\cos(b) & -j\sin(b) & 0\\ a & \dfrac{jb\sin(b)}{\varepsilon_{r1}} & \dfrac{b\cos(b)}{\varepsilon_{r1}} & 0\\ 0 & 1 & 0 & -\cos(d)\\ 0 & 0 & \dfrac{bh_2}{h_1\varepsilon_{r1}} & \dfrac{-jd\sin(d)}{\varepsilon_{r2}}\end{bmatrix}} \tag{12}$$

where $a=k_{0z}d_1=k_{0z}h_1$, $b=k_{1z}d_1=k_{1z}h_1$, $d=k_{2z}(d_2-d_1)=k_{2z}h_2$, N_m is the numerator of the reflection coefficient, and D_n is the denominator of the reflection coefficient. The relationships between a, b, and d are listed as follows:

$$b^2=(k_1^2-k_0^2)h_1^2+a^2 \tag{13}$$

$$d^2=(k_2^2-k_0^2)h_2^2+a^2h_2^2h_1^{-2}. \tag{14}$$

Let the denominator of R^{TM} be equal to zero, we get the mode (15). After doing some row and column operations, the mode equation f is explicitly in the form of an even function of k_{1z} and k_{2z}

$$f=\det(D_n)=\det\begin{bmatrix}1 & -\cos(b) & -jb\sin(b) & 0\\ a & \dfrac{jb\sin(b)}{\varepsilon_{r1}} & \dfrac{b^2\cos(b)}{\varepsilon_{r1}} & 0\\ 0 & 1 & 0 & -\cos(d)\\ 0 & 0 & \dfrac{b^2h_2}{h_1\varepsilon_{r1}} & \dfrac{-jd\sin(d)}{\varepsilon_{r2}}\end{bmatrix}=0. \tag{15}$$

1) Method I—Method for Small and Moderate Values of Roots: By using Taylor-series expansions for expanding the sine and cosine functions, we get polynomials of b and d of even orders for some matrix elements

$$\cos d=\sum_{n=0}^{\infty}c_nd^{2n} \tag{16}$$

and

$$d\sin d=\sum_{n=0}^{\infty}s_nd^{2n+2} \tag{17}$$

where $s_n=(-1)^n/(2n+1)!$, and $c_n=(-1)^n/(2n)!$

We can then transform every element of the determinant matrix D_n into a polynomial equation of a using the above relationships. Here we expand the element $D_n(4,4)$ as an illustration as follows:

$$\begin{aligned}&D_n(4,4)\\ &=-\frac{jd\sin(d)}{\varepsilon_{r2}}\\ &=-\frac{j}{\varepsilon_{r2}}\sum_{n=0}^{N_{\max}}s_nh_2^{2n+2}[(k_2^2-k_0^2)+h_1^{-2}a^2]^{n+1}\\ &=-\frac{j}{\varepsilon_{r2}}\sum_{n=0}^{N_{\max}}\sum_{k=0}^{n+1}s_n\binom{n+1}{k}h_2^{2n+2}h_1^{-2k}(k_2^2-k_0^2)^{n+1-k}a^{2k}.\end{aligned} \tag{18}$$

There are relationships between some elements inside the determinant matrix. For example, $D_n(2,3)=-b^2D_n(1,2)/\varepsilon_{r1}$ and $D_n(2,2)=-D_n(1,3)/\varepsilon_{r1}$. By noticing this, we can speed up the calculation of the polynomial coefficients in the determinant matrix.

We truncate the Taylor series at $N_{\max}$ and calculate the coefficients of the mode equation by polynomial multiplication (MATLAB function: conv). The Laplace's formula (19) is used to reduce the size of the determinant matrix recursively and to calculate the coefficients efficiently as follows:

$$\det(D_n)=\sum_{i=1;j=1,2,3,4}(-1)^{i+j}D_n(i,j)D_n^*(i,j) \tag{19}$$

where $D_n^*(i,j)$ is the determinant of the matrix that results from D_n by removing the ith row and the jth column.

The Taylor-series expansions are applied to the sine and cosine functions and have infinite radii of convergence in the complex plane. Since the integrand is an even function of the k_{iz}'s of intermediate layers, there is no usual branch point square root when combined with Taylor-series expansions. All the modes for small and moderate values of a can be found by solving the polynomial mode equation using the numerical eigenvalue method. Let the absolute value of the largest root obtained from this Taylor expansion method be $a_{\max}$. In order to ensure all the surface wave modes are found in method I, we need to set the appropriate value for $N_{\max}$ to let $a_{\max}^2 > h_1^2(k_{1z}^2 - k_{0z}^2)$.

In actual implementation, we adopt this procedure to calculate the first 20 to 30 modes, including all the surface wave modes, lower order leaky wave, and improper modes by using a finite summation in the Taylor-series expansion. The higher order leaky wave and improper modes, approximately 150 of them, are calculated by method II, the asymptotic approach.

2) Test and Refinement of the Roots: To verify the roots, we substitute them back into the mode equation and check whether (15) is satisfied. Those that satisfy (15) will be kept for refinement by the Newton–Raphson method. The roots $a^{(0)}$ generated by method I will be used as initial values for refinement iteration. The equation for refinement iteration is shown as follows:

$$a^{(n+1)} = a^{(n)} - \frac{f(a^{(n)})}{\left(\frac{df}{da}\right)_{a=a^{(n)}}} \tag{20}$$

where

$$\frac{df}{da} = \det\begin{bmatrix} \frac{d(D_{n1})}{da} \\ D_{n2} \\ D_{n3} \\ D_{n4} \end{bmatrix} + \det\begin{bmatrix} D_{n1} \\ \frac{d(D_{n2})}{da} \\ D_{n3} \\ D_{n4} \end{bmatrix} + \det\begin{bmatrix} D_{n1} \\ D_{n2} \\ \frac{d(D_{n3})}{da} \\ D_{n4} \end{bmatrix} + \det\begin{bmatrix} D_{n1} \\ D_{n2} \\ D_{n3} \\ \frac{d(D_{n4})}{da} \end{bmatrix}.$$

The iteration is terminated by the following accuracy criteria:

$$\left| \frac{f(a^{(n)})}{a^{(n)}\left(\frac{df}{da}\right)_{a=a^{(n)}}} \right| \le 10^{-6}. \tag{21}$$

3) Method II—Method for Large Values of Roots: For large values of roots, which only include leaky wave modes and improper modes, we have asymptotic solutions initially,

$$a_l^{(0)} = \sqrt{(k_0^2 - k_2^2)d_1^2 + (p_0 + m\pi)^2 d_1^2 d_2^{-2}}$$

where

$$p_0 = \sqrt{(k_2^2 - k_0^2)d_2^2 + a_{\max}^2 d_2^2 d_1^{-2}}$$
$$m = 1, 2, 3, 4, 5 \ldots$$

and

$$a_{\max} \text{ is the largest root from method I.} \tag{22}$$

We then use the Newton–Raphson method to refine the roots. With these two complementary methods, methods I and II, all the modes corresponding to small, moderate, and large roots on the complex plane can be found. These procedures, which also include the space-independent part of the residues calculations, are required to be computed only once as pre-processing for all distances applications. The complete set of exact root locations is particularly important to ensure the accuracy of the spatial Green's functions at the intermediate source-to-field distance $0.02\lambda_0 < \rho < 0.05\lambda_0$.

4) Lossy Dielectrics and Lossy Conductor Case: For the case of lossy dielectrics, we first find the roots of the lossless case. We then proceed with a refinement process for lossy dielectrics and lossy conductor case by using the lossless mode locations as initial values. When using a lossy conductor as the GND, we need to change the boundary condition at interface $-d_2$. The electric field and magnetic field on the tangential direction in Region 2 and Region t are presented as follows.

Region 2:

$$E_{2\rho}(\rho) = \frac{jIl}{8\pi\omega\varepsilon_2}\int_{-\infty}^{\infty} dk_\rho \{Cj\sin[k_{2z}(z+d_2) + D\cos[k_{2z}(z+d_2)]\} \cdot \frac{k_{2z}k_\rho^2}{k_{0z}} H_1^{(2)}(k_\rho\rho) \tag{23}$$

$$H_{2\phi}(\rho) = -\frac{jIl}{8\pi}\int_{-\infty}^{\infty} dk_\rho \{C\cos[k_{2z}(z+d_2)] + Dj\sin[k_{2z}(z+d_2)]\} \cdot \frac{k_\rho^2}{k_{0z}} H_1^{(2)}(k_\rho\rho). \tag{24}$$

Region t

$$E_{t\rho}(\rho) = \frac{jIl}{8\pi\omega\varepsilon_t}\int_{-\infty}^{\infty} dk_\rho \{T^{\mathrm{TM}}\exp[jk_{tz}(z+d_2)]\}\frac{k_{tz}k_\rho^2}{k_{0z}} H_1^{(2)}(k_\rho\rho) \tag{25}$$

$$H_{t\phi}(\rho) = -\frac{jIl}{8\pi}\int_{-\infty}^{\infty} dk_\rho \{T^{\mathrm{TM}}\exp[jk_{tz}(z+d_2)]\}\frac{k_\rho^2}{k_{0z}} H_1^{(2)}(k_\rho\rho). \tag{26}$$

By matching the boundary conditions at the interface $-d_1$ and $-d_2$, we get the following four equations to replace (8)–(11):

$$\begin{cases} A - \cos[k_{2z}(d_2-d_1)]C - j\sin[k_{2z}(d_2-d_1)]D = 0 & (27) \\ \frac{k_{1z}}{\varepsilon_1}B - \frac{k_{2z}}{\varepsilon_2}j\sin[k_{2z}(d_2-d_1)]C - \frac{k_{2z}}{\varepsilon_2} \cdot \cos[k_{2z}(d_2-d_1)]D = 0 & (28) \\ C - T^{\mathrm{TM}} = 0 & (29) \\ \frac{k_{2z}}{\varepsilon_2}D - \frac{k_{tz}}{\varepsilon_t}T^{\mathrm{TM}} = 0. & (30) \end{cases}$$

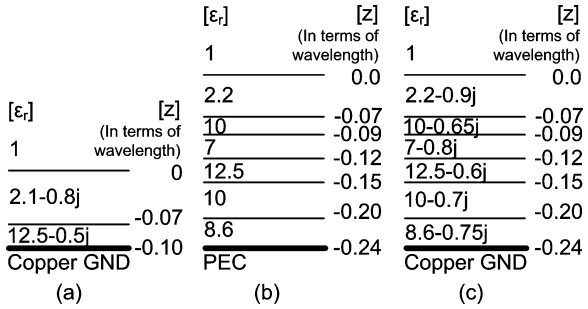

Fig. 2. (a) Case I: two-layer lossy media above a lossy copper GND. (b) Case II: six-layer lossless media above a PEC. (c) Case III: six-layer lossy media above a lossy copper GND.

Since the unknown T^{TM} is equal to C, there are five equations containing five unknowns, i.e., R^{TM}, A, B, C, and D. The mode equation for a two-layer substrate above a lossy conductor is shown in (31) at the bottom of this page, where $e = k_{tz}h_2 = \sqrt{(\varepsilon_{rt}-1)k_0^2h_2^2 + a^2h_2^2h_1^{-2}}$

Thus, we are able to include both lossy dielectric constants of the substrates and finite conductivity of the GND ($\sigma = 5.98 \times 10^7$ Sm^{-1} for copper in this case). The initial values of the roots, which generated from the lossless case, will be inserted into (31) for further refinement.

For the two-layer lossy problem, Case I of Fig. 2, the determination of the locations of up to 100 modes on the entire complex plane using method I and II requires CPU time of 0.569 s. (see Table I, row 2). Due to the accurate root locations generated from the two complementary methods, the further refinement using the Newton–Raphson method for the lossy case converges fast and takes less than 15 iterations to meet the accuracy criteria.

TABLE I
SOME SIMULATION RESULTS FOR DIFFERENT CASES

	Case I	Case II	Case III
CPU for FAM pre-processing (sec.)	0.569	1.361	2.265
N_S: number of surface wave modes	1	2	2
Number of Gauss-Hermite quadratures for very near field $\rho < 0.02\lambda_0$	3	3	3
Number of Gauss-Hermite quadratures for far field $\rho > 2\lambda_0$	4	4	4

5) Extension to Medium With an Arbitrary Number of Layers: The advantage of using the determinant format for the mode equation is that it can be readily extended to the problem with an arbitrary number of layers. For example, if we extend from a two-layer problem to a six-layer problem, we just add four more intermediate interfaces between top interface $-d_1$ and bottom interface $-d_n$. From them, we get two equations by matching boundary condition at each interface. They are of the same format as (27) and (28). The general mode equation for the N-layer problem above a lossy conductor is provided below with $2N+1$ number of equations containing $2N+1$ number of unknowns, shown in (32) at the bottom of this page, where $K_i = k_{iz}h_i$, $i = 1, 2, 3, \ldots, N$, $K_t = \sqrt{(\varepsilon_{rt}-1)k_0^2h_N^2 + a^2h_N^2h_1^{-2}}$ and

$$D_n(2i-1:2i+2, 2i:2i+1) = \begin{bmatrix} -\cos(K_i) & -j\sin(K_i) \\ \dfrac{jK_i\sin(K_i)}{-\varepsilon_{ri}} & \dfrac{K_i\cos(K_i)}{-\varepsilon_{ri}} \\ 1 & 0 \\ 0 & \dfrac{K_ih_{i+1}}{\varepsilon_{ri}h_i} \end{bmatrix}.$$

$$f = \det(D_n) = \det\begin{bmatrix} 1 & -\cos(b) & -j\sin(b) & 0 & 0 \\ a & \dfrac{jb\sin(b)}{\varepsilon_{r1}} & \dfrac{b\cos(b)}{\varepsilon_{r1}} & 0 & 0 \\ 0 & 1 & 0 & -\cos(d) & -j\sin(d) \\ 0 & 0 & \dfrac{bh_2}{\varepsilon_{r1}h_1} & \dfrac{-jd\sin(d)}{\varepsilon_{r2}} & \dfrac{-d\cos(d)}{\varepsilon_{r2}} \\ 0 & 0 & 0 & \dfrac{e}{\varepsilon_{rt}} & \dfrac{-d}{\varepsilon_{r2}} \end{bmatrix} = 0 \tag{31}$$

$$f = \det(D_n)_{(2N+1)\times(2N+1)} = \det\begin{bmatrix} 1 & -\cos(K_1) & -j\sin(K_1) & 0 & \ldots & 0 & 0 \\ -a & \dfrac{jK_1\sin(K_1)}{-\varepsilon_{r1}} & \dfrac{K_1\cos(K_1)}{-\varepsilon_{r1}} & 0 & \ldots & 0 & 0 \\ 0 & 1 & 0 & \ddots & \ddots & 0 & 0 \\ 0 & 0 & \dfrac{K_1h_2}{\varepsilon_{r1}h_1} & \ddots & \ddots & 0 & 0 \\ \vdots & \vdots & 0 & \ddots & \ddots & -\cos(K_N) & -j\sin(K_N) \\ 0 & 0 & 0 & \ddots & \ddots & \dfrac{jK_N\sin(K_N)}{-\varepsilon_{rN}} & \dfrac{K_N\cos(K_N)}{-\varepsilon_{rN}} \\ 0 & 0 & 0 & 0 & 0 & \dfrac{K_t}{\varepsilon_{rt}} & \dfrac{jK_N\sin(K_N)}{-\varepsilon_{rN}} \end{bmatrix} = 0 \tag{32}$$

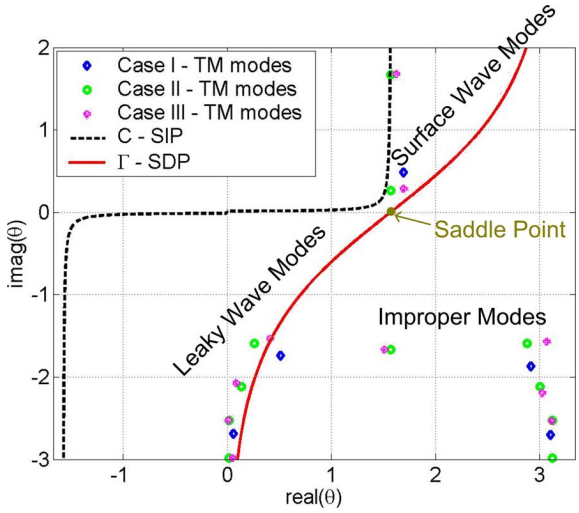

Fig. 3. SIP, SDP, and mode locations for all three cases on a complex θ plane.

Using $k_\rho = k_0 \sin\theta$ and $k_{0z} = k_0 \cos\theta$, we illustrate the locations of modes in the complex θ plane in Fig. 3. The lossy substrate shifts the locations of the surface wave modes away from the $\theta = \pi/2$ axis. The number of surface wave poles increases when increasing the thickness of the dielectric substrate (see Table I, row 3).

B. NMSP Including Effects of all Modes for Nonnear Field $\rho > 0.02\,\lambda_0$

We can map the vertical branch cuts of k_{0z} from the complex k_ρ plane to the complex θ plane [19]. We labeled the SIP by C. The SDP is labeled Γ and defined by $\mathrm{Re}(\sin\theta) = 1$ (Fig. 3).

The NMSP consists of the integration over Γ and the summation of residues from all proper modes, including the surface wave modes and leaky wave modes, which are located between C and Γ

$$E_{0z} = -\frac{Il}{8\pi\omega\varepsilon_0}[Q_{0z}^{\Gamma} - 2\pi j \sum_p R_{k_{\rho p}}] \tag{33}$$

where Q_{0z}^{Γ} is the integration along the Γ, and $R_{k_{\rho p}}$ is the residue of mode p between C and Γ.

The calculation of the residues is as follows:

$$R_{k_{\rho p}} = \frac{{k_{\rho p}}^3}{k_{0z}} H_0^{(2)}(k_{\rho p}\rho) \frac{\det[N_m(k_{\rho p})]}{\left\{\dfrac{d\det[D_n(k_\rho)]}{dk_\rho}\right\}_{k_\rho = k_{\rho p}}}. \tag{34}$$

Note that the denominators of the residues have already been calculated in the previous mode's refinement process. The calculations of residues are independent from the space-dependent factor $H_0^{(2)}(k_{\rho p}\rho)$. Since the wavenumber $k_{\rho p}$ of the leaky wave mode is a complex number, the Hankel function decays exponentially with ρ. Thus, we can use the criterion $|\mathrm{Im}(k_{\rho p})|\rho \le N_b$ to count the required number of leaky wave modes as ρ increases. In Table II, column 2, we list the number of leaky wave modes needed for the computation of the residues against different distances ρ.

TABLE II
NUMBER OF LEAKY WAVE MODES, NUMBER OF POLES FOR EXTRACTION, AND NUMBER OF TRAPEZOIDAL INTEGRATION POINTS NEEDED AT DIFFERENT DISTANCES FOR CASE III

Distance of ρ (in terms of λ_0)	N_L	N_X	N_I
0.02	37	77	52
0.05	15	32	38
0.2	3	9	30
0.5	1	5	16
1	0	1	14
3	0	1	12
10	0	1	10

To facilitate the integration along Γ, we further map Γ to the complex x-plane by $k_\rho = k_0 - jx^2/(2\rho)$. The mapping relationship between x and θ is

$$x = 2\exp\left(-\frac{j\pi}{4}\right)\sqrt{\rho k_0}\,\sin\left(\frac{\theta}{2} - \frac{\pi}{4}\right). \tag{35}$$

On the complex x-plane, Γ is along the real x-axis from $-\infty$ to $+\infty$. The integrand decreases from the saddle point ($x = 0$) in a Gaussian manner. Thus, we write Q_{0z}^{Γ} by the following equation:

$$Q_{0z}^{\Gamma} = \int_{-\infty}^{\infty} dx \Phi(x) \exp\left(-\frac{x^2}{2}\right) \tag{36}$$

where

$$\Phi(x) = -j\frac{x}{\rho}\exp\left(\frac{x^2}{2}\right)\left(1 + \frac{\det[N_m(x)]}{\det[D_n(x)]}\right) \cdot \frac{k_0^2 \sin^3\theta}{\cos\theta} H_0^{(2)}(k_0\rho\sin\theta).$$

When numerically integrating along the real x-axis, some modes can be very close to the saddle point. Those modes cause significant oscillation of the integrand. To smooth the integrand over the range between $-x_{\max}$ and $x_{\max}$, we adopt the NMSP with poles extraction, which was presented for a single-layer case in [1]. The NMSP can extract all the poles that are close to the saddle point, including not only proper modes, but also improper modes.

For a pole θ_p, we can get the x_p location on the x-plane through (35). In Fig. 4, we plot Γ and the pole locations for all three cases in the complex x-plane, where $\rho = 0.05\,\lambda_0$. We use $x_{\max} = 4.5$ and $N_b = 10$ in this paper. The closer the pole is to the saddle point, the stronger effect the pole contributes to the oscillation of the integrand. The distance between pole and saddle point in the complex x-plane is proportional to the square root of ρ. Therefore, when ρ increases, we require a lesser number of poles for the extraction. In Table II, column 3, we list the number of poles N_X needed for the extractions against different distances ρ.

The integrand along the SDP will decay faster at larger source-to-field distance ρ. Therefore, we need a lesser number of points for integration in the far-field region. In Table II, column 4, we list the number of trapezoidal integration points needed for different distances ρ. The reason we can use fewer than 60 trapezoidal integration points is that we have extracted all the nearby modes including the improper modes. Although the improper modes do not contribute to the residues, they

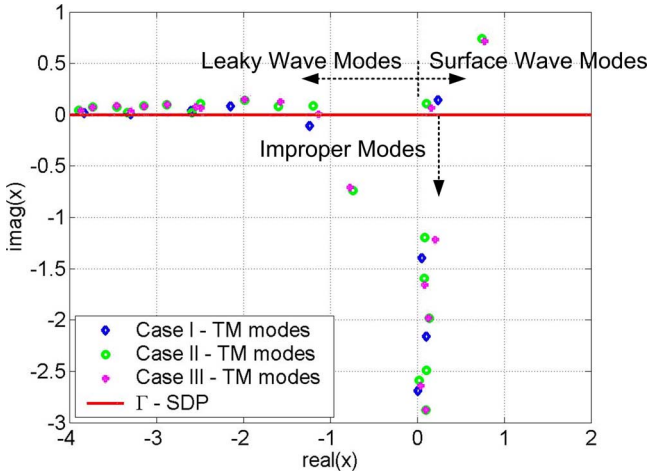

Fig. 4. SDP and modes locations for all three cases on the complex x-plane, where $\rho = 0.05\lambda_0$.

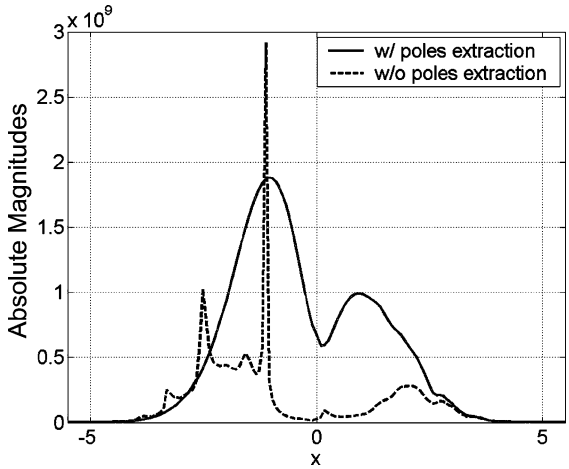

Fig. 5. Illustration of the large difference between the integrands over the SDP with and without extraction of the nearby poles for Case III, where $\rho = 0.05\lambda_0$.

have large effects on the smoothness of the SDP integrand. Fig. 5 illustrates the difference between the integrands of E_{0z} along the SDP with and without extraction of the poles. By examining the pole locations on Fig. 4, we can see that the significant oscillations on Fig. 5 are induced by the poles close to the saddle point.

C. Modified Half-Space Extraction Method for Very Near Field $\rho < 0.002\,\lambda_0$

For distances smaller than 0.02 free-space wavelength, the NMSP is still valid. However, for such short distances, it is more efficient to compute the layered medium Green's function by using the modified half-space extraction method [11], [20].

III. Numerical Results

In Table II, we listed numerical results for Case III.

- N_L Number of leaky wave modes needed for $|\mathrm{Im}(k_{\rho p})|\rho \leq 10$.
- N_X Number of poles extracted for the integration over SDP, $|x| \leq 4.5$.
- N_I Number of sampling points in the trapezoidal integration

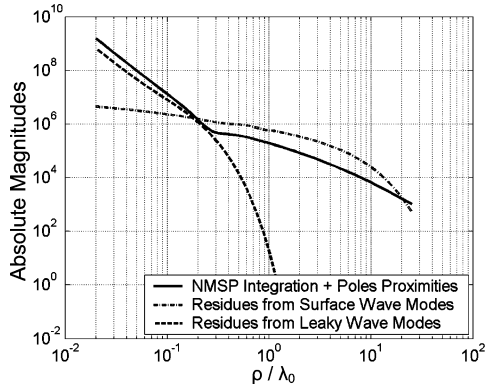

Fig. 6. Illustration of the magnitudes of the various contributions of electric field E_{0z} for case III.

TABLE III
CPU Time per Point for all Distance Ranges for E_{0z}

Range of ρ	Case I	Case II	Case III
$\rho < 0.02\lambda_0$ (near field)	0.443 msec.	0.541 msec.	0.595 msec.
$0.02\lambda_0 < \rho < 0.2\lambda_0$	5.965 msec.	6.545 msec.	7.546 msec.
$0.2\lambda_0 < \rho < 2\lambda_0$	2.982 msec.	4.782 msec.	4.891 msec.
$\rho > 2\lambda_0$ (far field)	1.792 msec.	2.621 msec.	2.624 msec.

For various distances of Case III, Table II shows that, as ρ increases, we need fewer modes for poles extraction, fewer points for integration, and fewer modes for residues calculation. Therefore, the NMSP requires less CPU time for larger ρ

As shown in Table I, row 5, in the far-field region, $\rho > 2\lambda_0$, we just need four Gauss–Hermite quadratures to complete the integration over the SDP, but the computation of the integration over the SDP is still necessary because for the lossy substrate case (Fig. 6), the energy of the surface waves decays exponentially with the distance ρ much faster than the decay of the contribution from the SDP. Thus, in the lossy case, the contribution from the SDP instead of from surface waves will dominate in the far-field region. However, in the lossless case, for distances over 50 free-space wavelength, the contribution from surface waves will dominate because the wavenumber $k_{\rho p}$'s of the surface wave modes are real numbers.

Note that, in the very near-field region $\rho < 0.02\lambda_0$, we use the modified half-space extraction method with Gauss–Hermite integration along the vertical branch cuts. Table I, row 4, shows the number of Gauss–Hermite quadratures we used for the very near-field region.

Table III shows the CPU of computing E_{0z} due to a VED in layered media for three cases on all ranges of ρ. All CPU times were taken on a P4 3.2-GHz PC running MATLAB. The FAM/NMSP method compute layered medium Green's functions for the range $0.02\ \lambda_0 \leq \rho \leq \infty$. The fast all modes pre-processing takes 2.265-s CPU time for computing the locations of 200 modes in Case III. Once the exact locations of all modes are determined, including surface wave modes, leaky wave modes, and improper modes, we can evaluate the layered medium Green's functions by fully exploiting the different types of poles according to their locations. For example, both surface wave poles and leaky wave poles contribute to the

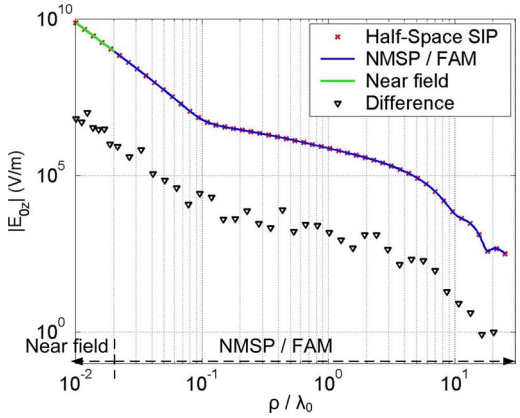

Fig. 7. $|E_{0z}|$ as a function of ρ due to a VED for Case I.

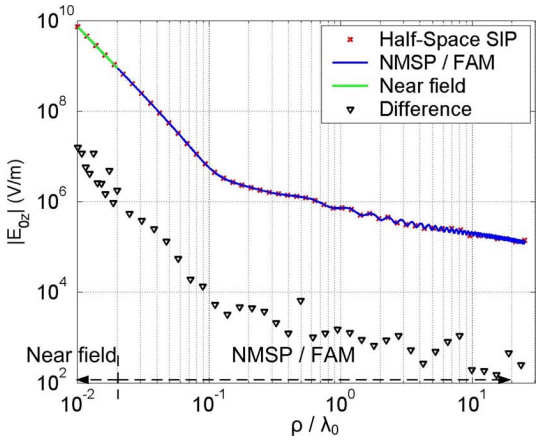

Fig. 8. $|E_{0z}|$ as a function of ρ due to a VED for Case II.

calculation of residues. All the proper and improper poles that are close to saddle point need to be extracted and replaced by error functions in the implementation of the NMSP. After the fast all modes pre-processing (Table II, row 2), the CPU per distance point in Table III covers the rest of the computation time, which consists of the summation of the N_S+N_L residues, the computation of the N_X incomplete error functions, and the N_I trapezoidal integration points. Within the context of 0.2% accuracy, the total CPU per point is less than 7.6 ms at any distance in Case III. Thus, to compute the fields at 1000 arbitrary distance points on the horizontal surface, for instance, the total CPU is $2.265 + 1000 \times 0.005 = 7.265$ s, assuming an average of 5 ms per point.

Figs. 7–9 show $|E_{0z}|$, the magnitudes of the multilayered spatial Green's functions for VED as a function of horizontal distance ρ ($0.01\lambda_0 < \rho < 25\lambda_0$) for Cases I–III, respectively. The solid blue line (in online version) is the result using the FAM/NMSP-based method, the cross red dot (in online version) is the result using the benchmark half-space extraction method, and the black triangle is the difference between these two methods. Comparison of the results using two methods confirms the accuracy of the FAM/NMSP method to within 0.2%. Note the triangles show that the differences are around 1000 times smaller than the actual values on the log scale plot.

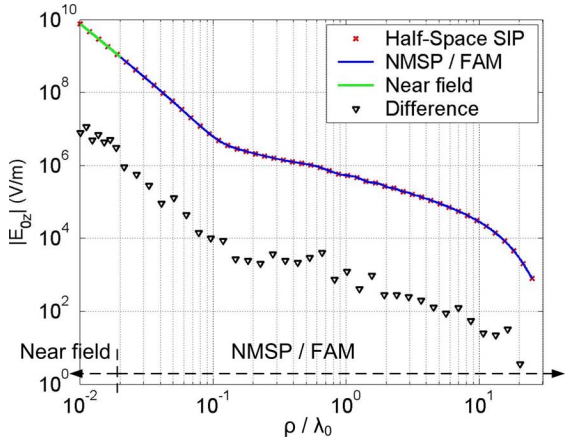

Fig. 9. $|E_{0z}|$ as a function of ρ due to a VED for Case III.

IV. Conclusion

In this paper, a fast and accurate approach, i.e., FAM/NMSP, has been presented to compute the spatial Green's functions of the multilayered problem with an arbitrary number of layers and lossy media for the entire distance range. We have presented the case when the source point and field point are on the surface, which is usually the most difficult case as the Sommerfeld integral is least convergent. We have systematically shown the technique and demonstrated the efficiency for the multilayer case of up to six layers with moderate total thicknesses, which is important for practical applications. The extension to lossy media over an imperfect conductor is also important because, in such a lossy condition, the surface waves no longer dominant in the far-field region. Accuracy within 0.2% is maintained for all these cases. We have already presented formulations and demonstrations for horizontal electric dipole (HED) on a lossless single layer substrate in [11]. We will continue our study of using the FAM/NMSP approach for other situations, e.g., vertical magnetic dipole (VMD), horizontal magnetic dipole (HMD), large numbers of multistack layers, dielectric GND, time-domain response, and negative index material in future research.

References

[1] L. Tsang and B. Wu, "Electromagnetic fields of Hertzian dipoles in layered media of moderate thickness including the effects of all modes," *IEEE Antennas Wireless Propag. Lett.*, vol. 6, no. 6, pp. 316–319, Jun. 2007.

[2] R. A. Kipp, C. H. Chan, A. T. Yang, and J. T. Yao, "Simulation of high frequency integrated circuits incorporating full wave analysis of microstrip discontinuities," *IEEE Trans. Microw. Theory Tech.*, vol. 41, no. 5, pp. 848–854, May 1993.

[3] C.-J. Ong, B. Wu, L. Tsang, and X. Gu, "Full-wave solver for microstrip trace and through-hole via in layered media," *IEEE Trans. Adv. Packag.*, vol. 31, no. 2, pp. 292–302, May 2008.

[4] V. N. Kourkoulos and A. C. Cangellaris, "Accurate approximation of Green's functions in planar stratified media in terms of a finite sum of spherical and cylindrical waves," *IEEE Trans. Antennas Propag.*, vol. 54, no. 5, pp. 1568–1576, May 2006.

[5] R. R. Boix, F. Mesa, and F. Medina, "Application of total least squares to the derivation of closed-form Green's functions for planar layered media," *IEEE Trans. Microw. Theory Tech.*, vol. 55, no. 2, pp. 268–280, Feb. 2007.

[6] Y. L. Chow, J. J. Yang, D. G. Fang, and G. E. Howard, "A closed-form spatial Green's function for the thick microstrip substrate," *IEEE Trans. Microw. Theory Tech.*, vol. 39, no. 3, pp. 588–592, Mar. 1991.
[7] M. I. Aksun and G. Dural, "Clarification of issues on the closed-form Green's functions in stratified media," *IEEE Trans. Antennas Propag.*, vol. 53, no. 11, pp. 3644–3653, Nov. 2005.
[8] E. Simsek, Q. H. Liu, and B. Wei, "Singularity subtraction for evaluation of Green's function for multilayer media," *IEEE Trans. Microw. Theory Tech.*, vol. 54, no. 1, pp. 216–225, Jan. 2006.
[9] M. Yuan, T. K. Sarkar, and M. Salazar-Palma, "A direct discrete complex image method from the closed-form Green's functions in multilayered media," *IEEE Trans. Microw. Theory Tech.*, vol. 54, no. 3, pp. 1025–1032, Mar. 2006.
[10] L. Tsang, C.-J. Ong, and B. Wu, "Electromagnetic fields of Hertzian dipoles in thin-layered media," *IEEE Antennas Wireless Propag. Lett.*, vol. 5, no. 12, pp. 537–540, Dec. 2006.
[11] B. Wu, L. Tsang, and C.-J. Ong, "Fast all modes (FAM) method combined with NMSP for evaluating spatial domain layered medium Green's functions of moderate thickness," *Microw. Opt. Technol. Lett.*, vol. 49, no. 12, pp. 3112–3118, Dec. 2007.
[12] M. Guglielmi and D. R. Jackson, "Low-frequency location of the leaky-wave poles for a dielectric layer," *IEEE Trans Microw. Theory Tech.*, vol. 38, no. 11, pp. 1743–1746, Nov. 1990.
[13] C.-I. G. Hsu, R. F. Harrington, J. R. Mautz, and T. K. Sarkar, "On the location of leaky wave poles for a grounded dielectric slab," *IEEE Trans Microw. Theory Tech.*, vol. 39, no. 2, pp. 346–349, Feb. 1991.
[14] M. A. Marin, S. Barkeshli, and P. H. Pathak, "On the location of proper and improper surface wave poles for the grounded dielectric slab," *IEEE Trans. Antennas Propag.*, vol. 38, no. 4, pp. 570–573, Apr. 1990.
[15] M. J. Neve and R. Paknys, "A technique for approximating the location of surface- and leaky- wave poles for a lossy dielectric slab," *IEEE Trans. Antennas Propag.*, vol. 54, no. 1, pp. 115–120, Jan. 2006.
[16] S.-A. Teo, M.-S. Leong, S.-T. Chew, and B.-L. Ooi, "Complete location of poles for thick lossy grounded dielectric slab," *IEEE Trans Microw. Theory Tech.*, vol. 50, no. 2, pp. 440–445, Feb. 2002.
[17] J. A. C. Weideman, "Computation of the complex error function," *SIAM J. Numer. Anal.*, vol. 31, pp. 1497–1518, 1994.
[18] L. Tsang, C.-C. Huang, and C. H. Chan, "Surface electric fields and impedance matrix elements of stratified media," *IEEE Trans. Antennas Propag.*, vol. 48, no. 10, pp. 1533–1543, Oct. 2000.
[19] L. Tsang and J. A. Kong, "Electromagnetic fields due to a horizontal electric dipole antenna laid on the surface of a two-layer medium," *IEEE Trans. Antennas Propag.*, vol. 22, no. 9, pp. 709–711, Sep. 1974.
[20] L. Tsang, C.-J. Ong, C.-C. Huang, and V. Jandhyala, "Evaluation of the Green's function for the mixed potential integral equation (MPIE) method in the time domain for layered media," *IEEE Trans. Antennas Propag.*, vol. 51, no. 7, pp. 1559–1571, Jul. 2003.
[21] L. M. Delves and J. N. Lyness, "A numerical method for locating the zeros of an analytic function," *Math. Comput.*, vol. 21, no. 100, pp. 543–560, Oct. 1967.
[22] A. G. Polimeridis, T. V. Yioultsis, and T. D. Tsiboukis, "A robust method for the computation of Green's functions in stratified media," *IEEE Trans. Antennas Propag.*, vol. 55, no. 7, pp. 1963–1969, Jul. 2007.

Boping Wu (S'04) received the B.Eng. degree (with first-class honors) in electronic and communication engineering from the City University of Hong Kong, Hong Kong, in 2005, the M.S. degree in electrical engineering from the University of Washington, Seattle, in 2007, and is currently working toward the Ph.D. degree at the University of Washington.

His current research interests include layered medium Green's functions, high-speed interconnects, microelectronic packaging, signal integrity, computation electromagnetics, metamaterials, and nanophotonics.

Leung Tsang (S'73–M'75–SM'85–F'90) received the S.B., S.M., and the Ph.D. degrees in electrical engineering and computer science from the Massachusetts Institute of Technology (MIT), Cambridge, in 1971, 1973, and 1976, respectively.

He is currently a Professor and Chair with the Department of Electrical Engineering, University of Washington, Seattle, where he has taught since 1983. From 2001 to 2004, he was on leave from the University of Washington, during which time he was with the Department of Electronic Engineering, City University of Hong Kong. He coauthored *Theory of Microwave Remote Sensing* (Wiley, 1985) and *Scattering of Electromagnetic Waves* (Wiley, 2000, 2001, 2001, vols. 1–3). His current research interests include remote sensing and geoscience applications, signal integrity of interconnects, computational electromagnetics, wireless communications and optoelectronics.

Dr. Tsang is a Fellow of the Optical Society of America. He was the president of the IEEE Geoscience and Remote Sensing Society for the 2006–2007 term. From 1996 and 2001, he was the editor-in-chief of the IEEE TRANSACTIONS ON GEOSCIENCE AND REMOTE SENSING. He is currently the chair of the IEEE TAB Periodicals Committee. He was the recipient of the 2000 IEEE Geoscience and Remote Sensing Society Outstanding Service Award and the 2000 IEEE Third Millennium Medal.